Automated subcellular localization and quantification of protein expression in tissue microarrays

ROBERT L. CAMP, GINA G. CHUNG & DAVID L. RIMM
Department of Pathology, Yale University School of Medicine, New Haven, Connecticut, USA
Correspondence should be addressed to D.L.R.; email: david.rimm@yale.edu

Published online 21 October 2002; doi:10.1038/nm791

The recent development of tissue microarrays—composed of hundreds of tissue sections from different tumors arrayed on a single glass slide—facilitates rapid evaluation of large-scale outcome studies. Realization of this potential depends on the ability to rapidly and precisely quantify the protein expression within each tissue spot. We have developed a set of algorithms that allow the rapid, automated, continuous and quantitative analysis of tissue microarrays, including the separation of tumor from stromal elements and the sub-cellular localization of signals. Validation studies using estrogen receptor in breast carcinoma show that automated analysis matches or exceeds the results of conventional pathologist-based scoring. Automated analysis and sub-cellular localization of beta-catenin in colon cancer identifies two novel, prognostically significant tumor subsets, not detected by traditional pathologist-based scoring. Development of automated analysis technology empowers tissue microarrays for use in discovery-type experiments (more typical of cDNA microarrays), with the added advantage of inclusion of long-term demographic and patient outcome information.

Despite the promise of automated analysis of histological sections, it has failed to replace traditional, pathologist-based evaluation, even in the simplest of conditions such as the analysis of immunohistochemical stains. Whereas the automated analysis of isolated cells in fluids or smears (for example, fluorescent cell sorting and laser scan cytometry) is now routine[1], the analysis of tissue sections is hampered by the fact that tumor tissue is a complex mixture of overlapping malignant tumor cells, benign host-derived cells and extracellular material. Several methods (including confocal and convolution/deconvolution microscopy) can determine the subcellular localization of target antigens, but only through computationally intensive techniques, requiring the acquisition of multiple high-power, serial images[2]. Methods designed for tissue microarrays perform only limited subcellular localization using morphometry and usually require significant manual interface (for example, drawing polygons around tumor cells)[3,4]. In general, pathologist-based analysis remains the current standard for the immunohistochemical studies.

Tissue microarrays provide a high-throughput method of analyzing the prognostic benefit of a myriad of potential targets on large cohorts of patient samples[5–7], but are limited by the pathologist's ability to reproducibly score on a continuous scale, discriminate between subtle low-level staining differences, and accurately score expression within subcellular compartments. We have developed a set of algorithms that we call AQUA (Automated Quantitative Analysis) that allow the rapid, automated analysis of large-scale cohorts on tissue microarrays. The first algorithm, called PLACE (pixel-based locale assignment for compartmentalization of expression) utilizes fluorescent tags to separate tumors from stroma and to define subcellular compartments. The distribution of a target antigen is then quantitatively assessed according to its co-localization with these tags. As subcellular compartments (for example, membrane, cytoplasm, nuclei and so forth) of different tissues and tumors vary widely in size and shape, traditional methods of defining compartments based on morphometric criteria (that is, feature extraction) perform poorly on a large-scale basis. Rather than counting target-containing features, PLACE delineates target expression as the sum of its intensity divided by the total size of the assayed compartment.

As the thickness of tissue sections makes it difficult to discriminate between overlapping subcellular compartments, we have also developed a novel, rapid exponential subtraction algorithm (RESA), which subtracts an out-of-focus image, collected slightly below the bottom of the tissue, from an in-focus image, based on pixel intensity, signal-to-noise ratio, and the expected compartment size. This algorithm dramatically improves the assignment of pixels to a particular subcellular compartment (Fig. 1). For a more complete discussion of the image manipulations performed in this protocol, see Supplementary Methods or http://www.yalepath.org/dept/research/YC-CTMA/tisarray.htm.

Validation of AQUA algorithms

Our initial validation of this technology compared its accuracy, intra-observer variability, and predictive power to traditional pathologist-based analysis. We stained a tissue microarray derived from 340 node-positive breast-carcinoma patients for the presence of estrogen receptor (ER)—the oldest and most common prognostic marker for breast cancer[8]. First we analyzed the ability of automated analysis to match results from a pathologist-based evaluation and found a high degree of correlation (R = 0.884, Fig 2*a*). Next, we compared the variability of a pathologist-based and automated analysis of two separate histospots derived from the same tumor (Fig. 2*b* and *c*). This comparison shows that automated analysis has slightly better reproducibility (R = 0.824 versus R = 0.732).

Although automated analysis compares favorably with pathologist-based interpretation of microarrays, the true criterion standard is outcome prediction. Estrogen receptor expression is known to significantly improve outcome, because it is associated with less aggressive tumors that are more responsive to anti-estrogenics (for example, Tamoxifen). We compared the survival of patients with tumors with high (top 25%) versus low (bottom 25%) ER expression as assessed by both automated and pathologist-based scoring (Fig. 2*d*). Results show that both methods provide similar prognostic information (RR = 2.44 versus 2.06, automated versus pathologist); although the auto-

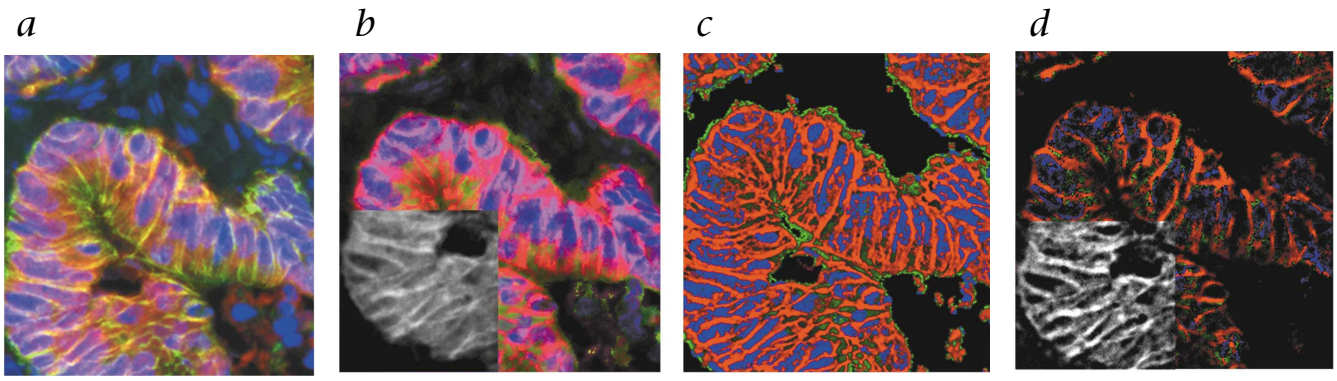

Fig. 1 RESA allows the accurate assignment of subcellular compartments and localization of a target antigen. ***a***, A pseudo three-color image of a colon carcinoma shows a significant degree of overlap between subcellular compartments: Blue, nuclei (DAPI); green, tumor mask (cytokeratin); red, tumor cell membranes (alpha-catenin). ***b***, The signal intensity of a target antigen, β-catenin (inset), is redistributed according to the relative signal intensity of the compartments identified in *a*: Blue, nuclear-localized; red, membrane-localized; green, cytoplasmic. Note that the β-catenin expression in this tumor is predominantly membrane-associated, yet there is significant incorrectly assigned signal in the nucleus: magenta and blue pixels. ***c***, The compartment-specific signals in *a* are reassigned using the RESA algorithm, reducing the amount of overlapping signal by exponentially subtracting pixel intensity from an out-of-focus image. ***d***, The signal intensity from an exponentially subtracted image of the target antigen, β-catenin (inset) is then redistributed according to the compartments defined in *c*. This results in more accurate assignment of the target antigen to the membrane compartment (red pixels) with little expression in the nuclear compartment (blue pixels).

mated analysis shows slightly higher significance ($P = 0.0003$ versus $P = 0.0020$). Univariate analysis of the automated analysis shows a relative risk of 2.438 ($P = 0.0005$, 95% CI 1.480–4.016). When analyzed in a multivariate analysis against histological and nuclear grades, age and stage, automated ER analysis retains independent prognostic significance ($RR = 2.566$, 95% CI 1.428–4.611, $P = 0.0016$). The pathologist-based analysis shows similar results, validating the cohort (see Supplementary Methods).

To determine the reproducibility of our automated analysis of ER, we used the 'split-sample technique,' by dividing the cohort into halves and using one half as a 'training' set and the other as a 'test' set[9]. The training set was used to determine standard cutoffs for the top and bottom 25% of cases. These cutoffs were then used to divide the test set into top, middle and bottom groups. We analyzed 300 randomly selected training and test sets; on average 97% of the test cases were correctly classified.

One clear advantage to automated analysis is that it can perform a true continuous assessment of a target. In contrast, the human eye, even that of a trained pathologist, has a difficult time accurately distinguishing subtle differences in staining intensity using a continuous scale. Consequently, scoring systems for pathologists tend to be nominal (for example, 0, 1+, 2+, 3+). Algorithms such as the 'H-score' are meant to translate such nominal observations into semi-quantitative results. However, the inability to detect subtle differences in staining intensity, particularly at the low and high ends of the scale, as well as the tendency to round scores limits the effectiveness of the H-score. The discontinuity of pathologist-based scoring, despite the use of an H-score algorithm, is exemplified in the

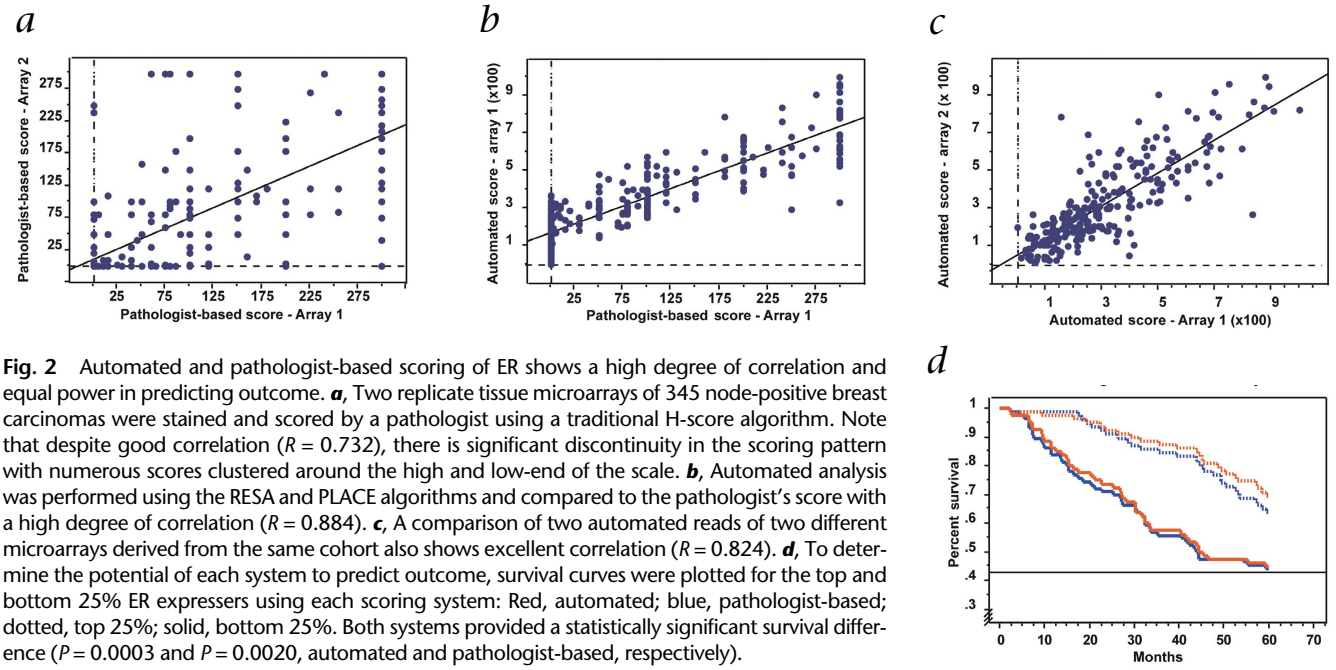

Fig. 2 Automated and pathologist-based scoring of ER shows a high degree of correlation and equal power in predicting outcome. ***a***, Two replicate tissue microarrays of 345 node-positive breast carcinomas were stained and scored by a pathologist using a traditional H-score algorithm. Note that despite good correlation ($R = 0.732$), there is significant discontinuity in the scoring pattern with numerous scores clustered around the high and low-end of the scale. ***b***, Automated analysis was performed using the RESA and PLACE algorithms and compared to the pathologist's score with a high degree of correlation ($R = 0.884$). ***c***, A comparison of two automated reads of two different microarrays derived from the same cohort also shows excellent correlation ($R = 0.824$). ***d***, To determine the potential of each system to predict outcome, survival curves were plotted for the top and bottom 25% ER expressers using each scoring system: Red, automated; blue, pathologist-based; dotted, top 25%; solid, bottom 25%. Both systems provided a statistically significant survival difference ($P = 0.0003$ and $P = 0.0020$, automated and pathologist-based, respectively).

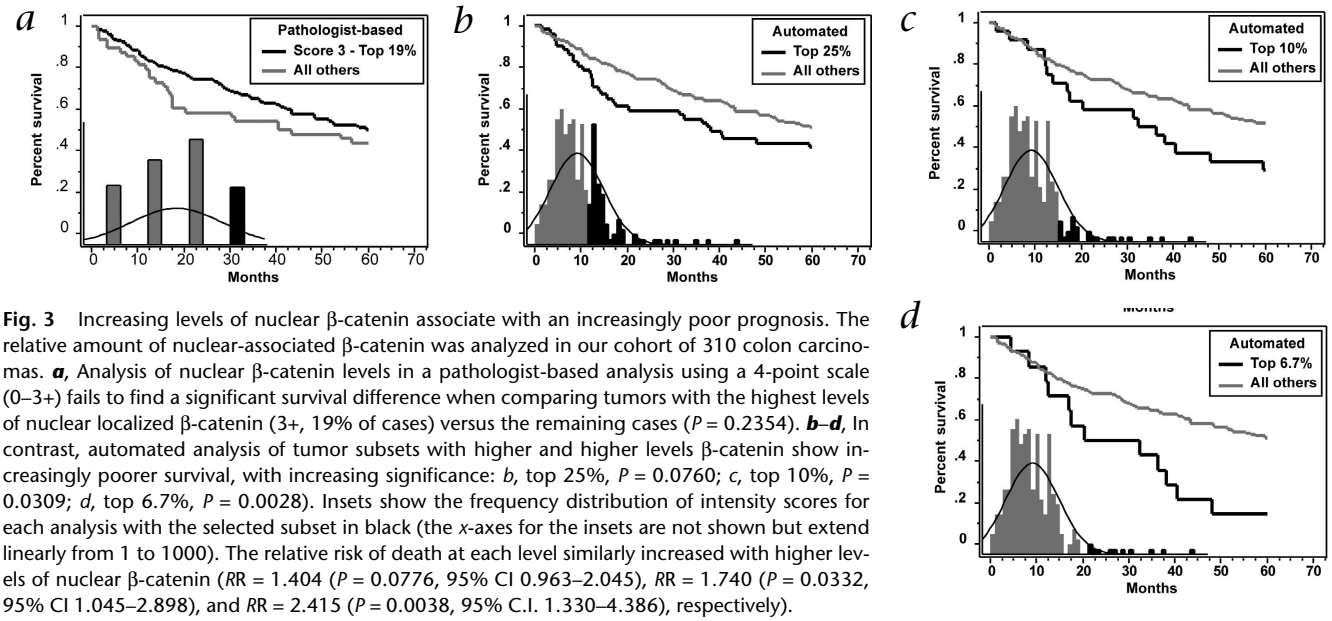

Fig. 3 Increasing levels of nuclear β-catenin associate with an increasingly poor prognosis. The relative amount of nuclear-associated β-catenin was analyzed in our cohort of 310 colon carcinomas. ***a***, Analysis of nuclear β-catenin levels in a pathologist-based analysis using a 4-point scale (0–3+) fails to find a significant survival difference when comparing tumors with the highest levels of nuclear localized β-catenin (3+, 19% of cases) versus the remaining cases ($P = 0.2354$). ***b***–***d***, In contrast, automated analysis of tumor subsets with higher and higher levels β-catenin show increasingly poorer survival, with increasing significance: *b*, top 25%, $P = 0.0760$; *c*, top 10%, $P = 0.0309$; *d*, top 6.7%, $P = 0.0028$). Insets show the frequency distribution of intensity scores for each analysis with the selected subset in black (the *x*-axes for the insets are not shown but extend linearly from 1 to 1000). The relative risk of death at each level similarly increased with higher levels of nuclear β-catenin (*RR* = 1.404 ($P = 0.0776$, 95% CI 0.963–2.045), *RR* = 1.740 ($P = 0.0332$, 95% CI 1.045–2.898), and *RR* = 2.415 ($P = 0.0038$, 95% C.I. 1.330–4.386), respectively).

ER staining results in Fig. 2. Note the preponderance of scores at 0, 100, 200 and 300. Furthermore, on average, over half of the cases were assigned to one extreme or the other (39% at 0 and 12% at 300). Thus 51% of the cases could not be effectively ranked. In contrast, the range of scores from the automated analysis is continuous from 0 to 1000. We hypothesize that the two key advantages of automated assessment, continuity of scoring and accurate subcellular localization, will allow tumor classification beyond that attainable by current methods.

Compartmental analysis of beta-catenin expression

To demonstrate this potential, we analyzed β-catenin expression in colon cancer. β-catenin is an ideal candidate in that it exhibits complex subcellular localization and manifests oncogenic properties upon localization to the nucleus[10]. Numerous studies have shown that β-catenin plays a dual role in both cell–cell adhesion and cell proliferation, depending on its location[11]. Membrane-associated β-catenin stabilizes cadherins-mediated adhesion by facilitating the cytoskeletal attachment of adhesion complexes. In contrast, nuclear-associated β-catenin activates several genes important in cell proliferation and invasion[12]. In development, translocation of β-catenin to the nucleus results from *wnt*-mediated cell signaling[13]. However, spurious activation of this pathway is often seen in tumors through mutation of β-catenin or other proteins involved in its activation and/or degradation[14]. Studies on the prognostic value of β-catenin have been mixed[15–17].

The complex biology and uncertain prognostic value of β-catenin made it a suitable candidate for assessing the value of quantitative subcellular localization. We studied a cohort of 310 colon cancers, using both pathologist-based and automated systems for scoring overall, nuclear and membrane-associated levels of β-catenin expression. Manual analysis used a traditional 4-point nominal scale (0 through 3+), whereas automated analysis used a continuous 1,000-point scale. In a previous study using a similar cohort, we were unable to find prognostic value in assessing nuclear β-catenin levels[18]. These data were confirmed in our present study when comparing tu-

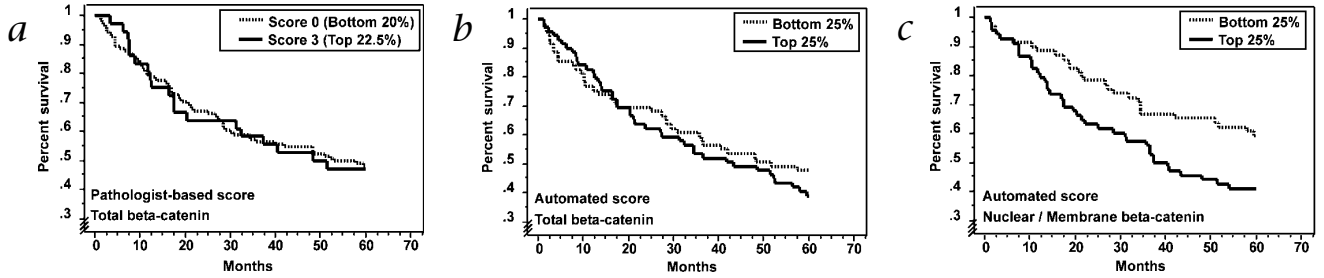

Fig. 4 Unlike analyses of overall β-catenin expression, automated, subcellular localization of β-catenin can predict outcome in colon carcinoma. ***a***, Overall β-catenin levels in a cohort of 310 colon cancers were evaluated by a pathologist using a 4-point scale (0–3+). Survival analysis of tumors with the lowest (0) versus highest (3+) overall β-catenin expression was not significant ($P = 0.9425$). ***b***, Similarly, automated analysis of overall β-catenin levels, comparing cases in the top and bottom 25%, failed to detect a survival difference ($P = 0.4551$). ***c***, In contrast, the ratio of nuclear to membrane β-catenin, as assessed by automated analysis, demonstrates that tumors with higher relative nuclear expression do worse than those with higher relative membrane expression ($P = 0.0264$, top versus bottom 25% of cases, *RR* = 1.718, 95% CI = 1.059–2.787). Note that the nuclear/membrane ratio identifies a large subset (25%) of tumors with poor prognosis, the majority of which are not identified by analyzing individual subcellular compartments. Indeed, comparison of tumors with high nuclear/membrane ratios (top 25%) versus those with high nuclear β-catenin (top 25%) shows that there is only 47% overlap.

mors expressing the highest levels of nuclear β-catenin (3+, representing 19% of the cases) versus the rest (Fig 3*a*) (P = 0.2354). We hypothesized that with the benefit of automated, continuous assessment, these 3+ cases could be subdivided into cases expressing very high versus high levels. We began by analyzing the top 25% of tumors expressing nuclear β-catenin, as assessed by automated analysis. This group shows a trend toward poorer survival (Fig 3*b*) (P = 0.0760). When we subset the tumors to assess the top 10% expressers, there is a statistically significant survival difference (Fig. 3*c*) (P = 0.0332, relative risk = 1.740). Further fractionation of the data reveals that the top 6.7% (15th percentile) exhibit even poorer survival with a higher statistical significance (Fig. 3*d*) (P = 0.0038, relative risk = 2.415). This analysis demonstrates the power of continuous automated assessment to define subsets of tumors not seen using standard pathologist-based assessment. Unlike β-catenin, subdividing ER into smaller and smaller subsets does not significantly alter its prognostic ability, suggesting that ER may be a truly continuous marker where no subpopulations exist.

Tumor classification using the AQUA algorithms

We then attempted a tumor classification based on comparative subcellular localization. As the translocation of β-catenin from the membrane to the nucleus is thought to correlate with transcriptional activation, we analyzed the ratio of nuclear to membrane-localized β-catenin. By its nature, this type of analysis is essentially impossible without continuous scoring. A crude measurement of overall β-catenin levels using either a pathologist-based or an automated system fails to demonstrate a significant difference in survival between the highest and lowest expressing tumors (Fig. 4, *a* and *b*, P = 0.9425 and P = 0.4551, respectively). In contrast, when we ratio the level of nuclear/membrane β-catenin, we find that tumors with a high ratio have a worse outcome than tumors with a low ratio (RR = 1.718, P = 0.0284). Note that this method defines a relatively large subset (25%) of tumors with poor prognosis, the majority of which are not identified by analyzing individual subcellular compartments. Indeed, a comparison of the tumors with the highest nuclear/membrane ratio (top 25%) versus the highest overall nuclear levels of β-catenin (top 25%) shows that there is only 47% overlap between the two subsets. Multivariate analysis of nuclear/membrane β-catenin ratios shows independent prognostic significance when analyzed with depth of invasion, nodal status, tumor grade and patient age (RR = 1.865, 95% CI = 1.068–3.259, P = 0.0285). In contrast, multivariate analysis of total nuclear β-catenin levels fails to show independent prognostic significance because it is highly correlated with nodal metastases (see Supplementary Methods online).

The methods presented here are highly adaptable to a number of tumor types and target markers. In most cases, compartment-specific tags are identical regardless of tumor type (DAPI for nuclei, cadherins/catenin complexes for membranes). Because the methods do not use heuristic models that require recognition of compartments according to size, shape or texture, they are fully adaptable to tumors with overlapping or pleomorphic cells and/or nuclei. Furthermore, the algorithms can be easily expanded to cover novel compartments or even 'virtual' compartments (for example, mitochondria, lysosomes, cortical actin ring) or tumor types (for example, mesothelioma), as long as tags can be identified for the prospective compartments/cell types. In addition to ER and β-catenin, we have used these techniques to successfully analyze dozens of markers, including growth factor receptors, intracellular signaling molecules, and proliferation markers, using both conventional and phospho-specific antibodies (see Supplementary Methods online). Analysis of these targets requires only a standard antibody titration.

We have found that most antigens benefit from subcellular localization. Localization can be simple, such as determining the amount of the proliferation marker KI-67 in tumor nuclei, or more complex as in the case of β-catenin. Localization of intracellular signaling molecules (for example, STATs) may be vital in assessing their potential as prognostic markers. In addition, recent studies have shown that membrane-bound growth factor receptors (for example, epidermal growth factors, EGFR and ERB-B4, and fibroblast growth factor) can translocate to the nucleus and may act as transcriptional regulators[19]. Subcellular localization of such markers may be critical to their use as prognostic markers in cancer.

Depending upon the array size, and the complexity of the compartmentalization, analyses using our current device take from 1–3 hours for image acquisition, and 1–2 hours for analysis. In our laboratory, the average pathologist-based analysis rate is 50–100 spots per hour and usually is performed in several sessions. To increase precision, two or more pathologists read the same array independently and then together to resolve discrepancies. Aside from being more accurate and more robust, automated analysis can be performed continuously and results tabulated immediately. We estimate that a fully integrated tissue microarray reader could be 30 to 50 times faster than pathologist-based scoring.

Methods

Tissue microarray design and processing. Paraffin-embedded formalin-fixed specimens from 345 cases of node-positive breast carcinoma (1962–1977) and 310 cases of colon carcinoma (1971–1982) were obtained, as available, from the archives of the Yale University Department of Pathology. Microarray slides were prepared, processed and stained as described in the Supplementary Methods online. For manual analysis, slides were visualized with diaminobenzidine (DAB). For automated analysis, slides were visualized with Cy-5 tyramide.

Image and data analysis. Monochromatic images of tissue microarray histospots were obtained using fluorescently labeled compartment specific tags (anti-cytokeratin, DAPI, α-catenin) as well as target signals (ER and β-catenin). Regions of tumor were identified using a mask derived from a ubiquitously expressed epithelial-specific antigen (either cytokeratin or α-catenin). Images were analyzed using RESA and PLACE algorithms as detailed in the Supplementary Methods online. Results were expressed as the intensity of the target signal in each compartment divided by the compartment. For ER, only nuclear-localized signal was used; for β-catenin total signal, the ratios of nuclear-to-membrane signal and nuclear-to-total signal were analyzed. Overall survival analysis was assessed using Kaplan–Meier analysis and the Mantel–Cox log-rank score for assessing statistical significance. Relative risk was assessed using the univariate and multivariate Cox-proportional hazards model.

Our data show that quantitative, continuous-scale, compartmentalized automated analysis of tissue microarrays can provide a rapid assessment of prognosis-based subsets in a variety of tumor markers that cannot be attained using pathologist-based techniques. Automated analysis is better able to discern subtle differences in staining intensity, particularly at the upper and lower extremes, which can distinguish novel prognostic associations. Furthermore, analysis of the subcellular distribution of certain signals, using the PLACE and RESA algorithms may elucidate previously unrecognized associations with patient survival. The automated nature of this technology can allow high-throughput screening of tissue microarrays, facilitating their use in large-scale, high-throughput applications such as target discovery and prognostic marker validation. If, someday, diagnostic criteria are based on molecular expression patterns, the digital nature of this analysis could allow a device of this type to make specific molecular diagnoses.

Note: Supplementary information available on the Nature Medicine *website.*

Acknowledgments

We thank T. D'Aquila, M. Helie, L. Charette, D. Fischer, E. Rimm and P. Lizardi for their help in this effort; and J. Costa, V. Marchesi, A. Reynolds, R. Levenson and E. Fearon for review of the manuscript. This work was supported by grants from the Patrick and Catherine Weldon Donaghue Foundation for Medical Research and grants from the NIH including: K0-8 ES11571, NIEHS (to R.L.C.), RO-1 GM57604 NCI (to D.L.R.) and US Army DAMD grant 01-000436.

Competing interests statement

The authors declare competing financial interests: see the website (http://nature.com/naturemedicine

1. Tarnok, A. & Gerstner, A.O. Clinical applications of laser scanning cytometry. *Cytometry* **50**, 133–143 (2002).
2. Robinson, J.P. Principles of confocal microscopy. *Methods Cell Biol.* **63**, 89–106 (2001).
3. Rao, J., Seligson, D. & Hemstreet, G.P. Protein expression analysis using quantitative fluorescence image analysis on tissue microarray slides. *Biotechniques* **32**, 924–932 (2002).
4. Bacus, S. *et al.* Potential use of image analysis for the evaluation of cellular predicting factors for therapeutic response in breast cancers. *Anal. Quant. Cytol. Histol.* **19**, 316–328 (1997).
5. Kallioniemi, O.P., Wagner, U., Kononen, J. & Sauter, G. Tissue microarray technology for high-throughput molecular profiling of cancer. *Hum. Mol. Genet.* **10**, 657–662 (2001).
6. Kononen, J. *et al.* Tissue microarrays for high-throughput molecular profiling of tumor specimens. *Nature Med.* **4**, 844–847 (1998).
7. Rimm, D.L. *et al.* Tissue microarray: a new technology for amplification of tissue resources. *Cancer J* **7**, 24–31 (2001).
8. Osborne, C.K. *et al.* Estrogen receptor, a marker for human breast cancer differentiation and patient prognosis. *Adv. Exp. Med. Biol.* **138**, 377–385 (1981).
9. Wasson, J.H., Sox, H.C., Neff, R.K. & Goldman, L. Clinical prediction rules. Applications and methodological standards. *N. Engl. J. Med.* **313**, 793–799 (1985).
10. Kobayashi, M. *et al.* Nuclear translocation of β-catenin in colorectal cancer. *Br. J. Cancer* **82**, 1689–1693 (2000).
11. Provost, E. & Rimm, D.L. Controversies at the cytoplasmic face of the cadherin-based adhesion complex. *Curr. Opin. Cell Biol.* **11**, 567–572 (1999).
12. Morin, P.J. β-catenin signaling and cancer. *Bioessays* **21**, 1021–1030 (1999).
13. Peifer, M. & Polakis, P. Wnt signaling in oncogenesis and embryogenesis—a look outside the nucleus. *Science* **287**, 1606–1609 (2000).
14. Wong, C.M., Fan, S.T. & Ng, I.O. β-catenin mutation and overexpression in hepatocellular carcinoma: clinicopathologic and prognostic significance. *Cancer* **92**, 136–145 (2001).
15. Gunther, K. *et al.* Predictive value of nuclear β-catenin expression for the occurrence of distant metastases in rectal cancer. *Dis. Colon Rectum* **41**, 1256–1261 (1998).
16. Maruyama, K. *et al.* Cytoplasmic β-catenin accumulation as a predictor of hematogenous metastasis in human colorectal cancer. *Oncology* **59**, 302–309 (2000).
17. Hugh, T.J. *et al.* Beta-catenin expression in primary and metastatic colorectal carcinoma. *Int. J. Cancer* **82**, 504–511 (1999).
18. Chung, G.G. *et al.* Tissue microarray analysis of β-catenin in colorectal cancer shows nuclear phospho-β-catenin is associated with a better prognosis. *Clin. Cancer Res.* **7**, 4013–4020 (2001).
19. Lin, S.Y. *et al.* Nuclear localization of EGF receptor and its potential new role as a transcription factor. *Nature Cell Biol.* **3**, 802–808 (2001).

Automated subcellular localization and quantification of protein expression in tissue microarrays

ROBERT L. CAMP, GINA G. CHUNG & DAVID L. RIMM
Department of Pathology, Yale University School of Medicine, New Haven, Connecticut, USA
Correspondence should be addressed to D.L.R.; email: david.rimm@yale.edu

Published online 21 October 2002; doi:10.1038/nm791

Supplemental Material

Materials and methods

Tissue microarray design and processing. Paraffin-embedded, formalin-fixed specimens from 345 cases of node-positive breast carcinoma (1962–1977) and 310 cases of colon carcinoma (1971–1982) were obtained, as available, from the archives of the Yale University, Department of Pathology. Areas of invasive carcinoma, away from *in situ* lesions and normal epithelium, were identified and two 0.6-mm cores were taken from separate areas. Each core was arrayed into recipient blocks in a 1mm-spaced grid covering approximately 1 square inch, and 5-micron thick sections were cut and processed as previously described[1].

Immunohistochemistry. In brief, pre-cut paraffin-coated tissue microarray slides were deparaffinized and antigen-retrieved by pressure-cooking[2]. Slides were preincubated with 0.3% bovine serum albumin in 0.1M tris-buffered saline (pH 8.0) (BSA/TBS) for 30 min at room temperature. Slides were then incubated with primary antibodies diluted in BSA/TBS either for 1 h at room temperature or overnight at 4 °C. Slides were washed 3x 5 min with BSA/TBS containing 0.05% Tween-20. Corresponding secondary antibodies were applied for 1 h at room temperature in BSA/TBS. These included either antibodies directly conjugated to a fluorphore (Amersham, Piscataway, New Jersey and Molecular Probes, Eugene, Oregon), and/or conjugated to a horseradish peroxidase (HRP) decorated dextran-polymer backbone (Envision, DAKO, Carpinteria, California). DAPI was included with the secondary antibodies to visualize nuclei. Slides were again washed 3x 5 min with BSA/TBS containing 0.05% Tween-20. For manual analysis, slides were then incubated with diaminobenzidine (DAB, DAKO). For automated analysis, slides were incubated with a fluorescent chromagen (Cy-5-tyramide, NEN Life Science Products, Boston, Massachusetts) which, like DAB, is activated by HRP and results in the deposition of numerous covalently associated Cy-5 dyes immediately adjacent to the HRP-conjugated secondary antibody. Cy-5 (red) was used because its emission peak is well outside the green-orange spectrum of tissue autofluorescence. Slides for automated analysis were coverslipped with an antifade-containing mounting medium (Gelvatol with 0.6% n-propyl gallate). Manual examination of microarrays for ER and β-catenin levels has been previously described[3].

Specifically, four sets of primaries and secondaries were used:
Estrogen receptor (manual analysis): Primary: mouse monoclonal anti-ER (1:1 of clinical pre-diluted antibody, DAKO) for 1 h. Secondary: Envision anti-mouse for 1 h. Chromagen for Envision antibody: diaminobenzidine. Counterstain: ammonium hydroxide acidified hematoxylin.
Estrogen Receptor (automated analysis): Primary: mouse monoclonal anti-ER (1:1 of clinical pre-diluted antibody, DAKO) for 1 h and polyclonal rabbit anti-cytokeratin (1:50, Zymed, South San Francisco, California) for 1 h as a cocktail. Secondaries: Alexa 488-conjugated goat anti-rabbit (1:200, Molecular Probes, Eugene, Oregon), Envision anti-mouse (neat) and DAPI for 1 h as a cocktail. Chromagen for Envision antibody: Cy-5 tyramide.
Beta-catenin (manual analysis): Primaries: monoclonal anti-β-catenin (mouse clone 14, BD Transduction Labs, San Diego California). Secondary: Envision anti-mouse for 1 h. Chromagen for Envision antibody: diaminobenzidine. Counterstain: ammonium hydroxide acidified hematoxylin.
Beta-catenin (automated analysis): Primaries: monoclonal anti-β-catenin (mouse clone 14, BD Transduction Labs) and polyclonal rabbit anti-α-catenin for 1 h. Secondaries: Alexa 488-conjugated goat anti-rabbit, Envision anti-mouse and DAPI for 1 h. Chromagen for Envision antibody: Cy-5 tyramide.

Image acquisition. Images of microarrays were obtained using a Deltavision platform and software (SoftWorx 2.5; Applied Precision, Issaquah, Washington), with an attached water-cooled Photometrics series 300 camera through a x10 Nikon Super-Fluor lens on a TE200 inverted fluorescent microscope with automated *x*, *y*, *z* stage movement. Low power images of microarrays were stitched together using multiple (~1500) low-resolution images of the microarray (64 x 64 pixel) at approximately 7-micron resolution. Histospots were identified using signal from DAPI, cytokeratin, or α-catenin tags. This signal was thresholded to create a binary image of the microarray. Histospots were identified using size criteria. Rows and columns of histospots were then identified, and missing histospots filled in, allowing each histospot to be identified based on its row/column grid position. The coordinates of each histospot were then recorded. Subsequently, monochromatic, high-resolution (1024 x 1024 pixel, 0.5-micron resolution) images were obtained of each histospot, both in the plane of focus and 8 microns below it, and recorded in an image stack as bitmaps. This depth, slightly below the bottom of the tissue, was determined to be optimal for 5-micron histologic sections. A resolution of 0.5 microns is suitable for distinguishing between large subcellular compartments such as the cell membrane and nuclei. In theory, smaller compartments (for example, mitochondria, nucleoli) might require higher resolution. Images were obtained using a dynamic range of 0–1024, but saved and analyzed as 8-bit tiff images with a dynamic range of 0–255.

RESA/PLACE algorithmic analysis of images. First, a tumor-specific mask is generated by thresholding the image of a marker that differentiates tumor from surrounding stroma and/or leukocytes. This creates a binary mask (each pixel is either 'on' or 'off'). In this study we used cytokeratin and α-catenin to create tumor masks. As formalin-fixed tissues can exhibit autofluorescence, analysis may give multiple background peaks. The RESA/PLACE algorithms determine which of these peaks is predominant and sets a binary mask threshold at a slightly higher intensity level. This provides an adaptive (unique to each histospot) thresholding system that ensures that only the target signal from the tumor and not the surrounding elements is analyzed. Thresholding levels were verified by spot-checking a few images and then automated for the remaining images. This binary mask can be modified using standard image manipulations. In most cases this involves filling holes of a particular size (for example, less than 500 pixels, to fill in tumor nuclei that do not stain for either cytokeratin or α-catenin) and removing extraneous single pixels. Once set, these image manipulations are performed automatically on all images. All subsequent image manipulations involve only image information from the masked area.

Next, two images (one in-focus, one slightly deeper) are taken of the compartment-specific tags and the target marker. A percent-

age of the out-of-focus image is subtracted from the in-focus image, based on a pixel-by-pixel analysis of the two images. This percentage is determined according to the ratio of the highest/lowest intensity pixels in the in-focus image – representing the signal-to-noise ratio of the image. By using an exponential scale, this allows RESA to subtract low intensity pixels in images with a low signal-to-noise ratio less heavily than low intensity pixels from images with a high signal-to-noise ratio. The overall degree of subtraction is based on a user-defined percentage for each subcellular compartment. For most applications this is empirically set to 40% of the total signal, and remains constant for images from an entire microarray. RESA thus eliminates all out-of-focus information. The algorithm has the added benefit of enhancing the interface between areas of higher intensity staining and adjacent areas of lower intensity staining, allowing more accurate assignment of pixels of adjacent compartments. In contrast to the compartment-specific tags, the RESA subtraction of the target signal is uniform and not based on overall intensity of the image intensity. This ensures that the same amount of subtraction occurs with the target signal from all specimens.

Finally, the PLACE algorithm assigns each pixel in the image to a specific subcellular compartment (Supplemental Figs. 1 and 2). Pixels that cannot be accurately assigned to a compartment to within a user-defined degree of confidence (usually 95%) are discarded. This is accomplished iteratively by determining the ratio of signal from two compartment-specific markers that minimizes the spillover of marker from one compartment into another. Pixels where the nuclear and membrane pixel intensities are too similar to be accurately assigned are negated (usually comprising <8% of the total pixels). A third compartment (the cytoplasm) can be defined by exclusion (non-membrane, non-nuclear). Once each pixel is assigned to a subcellular compartment (or excluded as described above), the signal in each location is added up. This data is saved and can subsequently be expressed either as a percentage of total signal or as the average signal intensity per compartment area. The score is expressed on a scale of 1 to 1000 as the total intensity detectable in a pixel ranges from 1–255 creating 3 significant figures. These algorithms are described in a recently submitted patent of this technology owned by Yale University. In this study, for ER, only nuclear-localized signal was used; for β-catenin total signal, the ratio of nuclear to membrane signal, and the ratio of nuclear to total signal was analyzed. Scores were adjusted according to amount of area covered by the subcellular compartments within the masked area

Data analysis. Staining scores from the breast cancer histospots represent the averaged results from two independently scored histospots. Histospot containing <10% tumor, as assessed either subjectively (manual) or by mask area (automated), were excluded from further analysis. For the purposes of validation, we did not manually exclude any images of histospots exhibiting aberrant staining (for example, with normal epithelium or in situ carcinoma), although such manual assessment could be performed. Our previous studies have demonstrated that scores from the average of two histospots matches the score from an entire tissue section >95% of the time[4]. Subsequent studies revealed that analysis of a single histospot could provide significant statistical power to judge outcomes (data not shown), so that staining scores from the colon cancer array represent the result of only one histospot. Estrogen receptor expression showed continuous prognostic significance such that virtually any division between low and high expressers resulted in a significant survival difference; therefore, we chose the top and bottom 25th percentiles as arbitrary divisions for high and low expression. Overall survival analysis was assessed using Kaplan-Meier analysis and the Mantel-Cox log-rank score for assessing statistical significance. Relative risk was assessed using the univariate and multivariate Cox-proportional hazards model (Tables 1–4). Analyses were performed using Statview 5.0.1 (SAS Institute, Cary, North Carolina).

1. Kononen, J. *et al*. Tissue microarrays for high-throughput molecular profiling of tumor specimens. *Nature Med.* **4**, 844–847 (1998).
2. Katoh, A.K., Stemmler, N., Specht, S. & D'Amico, F. Immunoperoxidase staining for estrogen and progesterone receptors in archival formalin fixed, paraffin embedded breast carcinomas after microwave antigen retrieval. *Biotech. Histochem.* **72**, 291–298 (1997).
3. Snead, D.R. *et al*. Methodology of immunohistological detection of oestrogen receptor in human breast carcinoma in formalin-fixed, paraffin-embedded tissue: a comparison with frozen section methodology. *Histopathology* **23**, 233–238 (1993).
4. Camp, R.L., Charette, L.A. & Rimm, D.L. Validation of tissue microarray technology in breast carcinoma. *Lab. Invest.* **80**, 1943–1949 (2000).

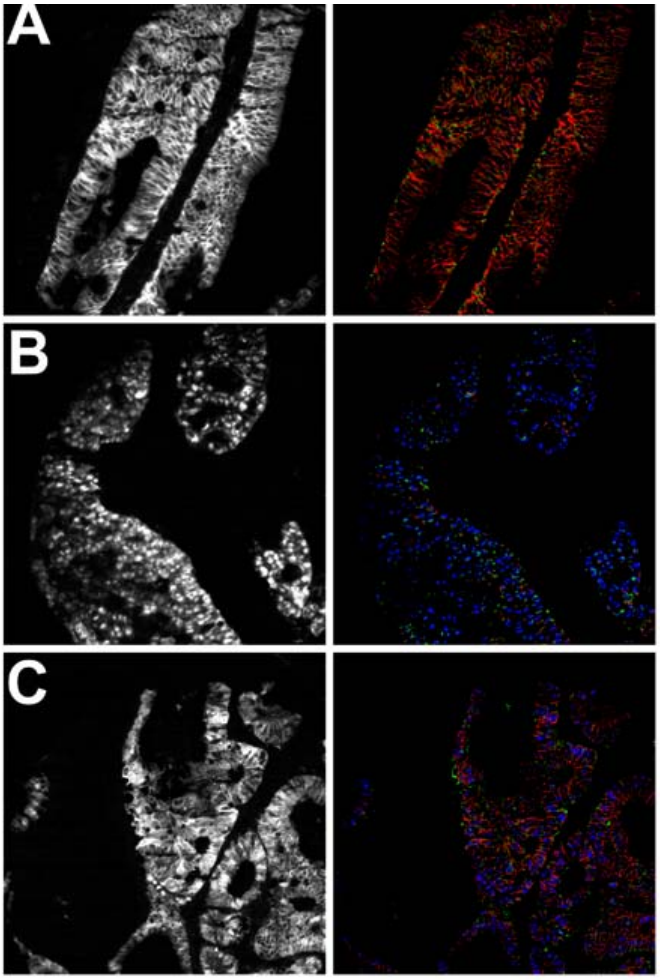

Fig. 1 Subcellular localization of β-catenin in three sample colon carcinomas. The importance of subcellular localization in automated analysis is exemplified by three colon carcinomas. An image of the carcinomas stained for β-catenin is shown of the left (grayscale), and the corresponding co-localization of that signal to subcellular compartments using RESA and PLACE is shown on the right (color). ***a***, Automated analysis of a colon carcinoma with predominantly membrane-associated β-catenin shows co-localization of the signal to the membrane (red) with little signal in the cytoplasm (green) or nuclei (blue). ***b***, Automated analysis of a carcinoma with predominantly nuclear-associated β-catenin shows co-localization of the signal to the nuclei (blue). ***c***, Automated analysis of a carcinoma with mixed β-catenin expression shows co-localization to both membrane (red), cytoplasmic (green) and nuclear (blue) compartments. Note that without subcellular localization, the overall expression of β-catenin in these three tumors would be similar. An additional confounding factor — the amount of surrounding desmoplastic stroma — is eliminated by using a mask (cytokeratin) that recognizes only tumor.

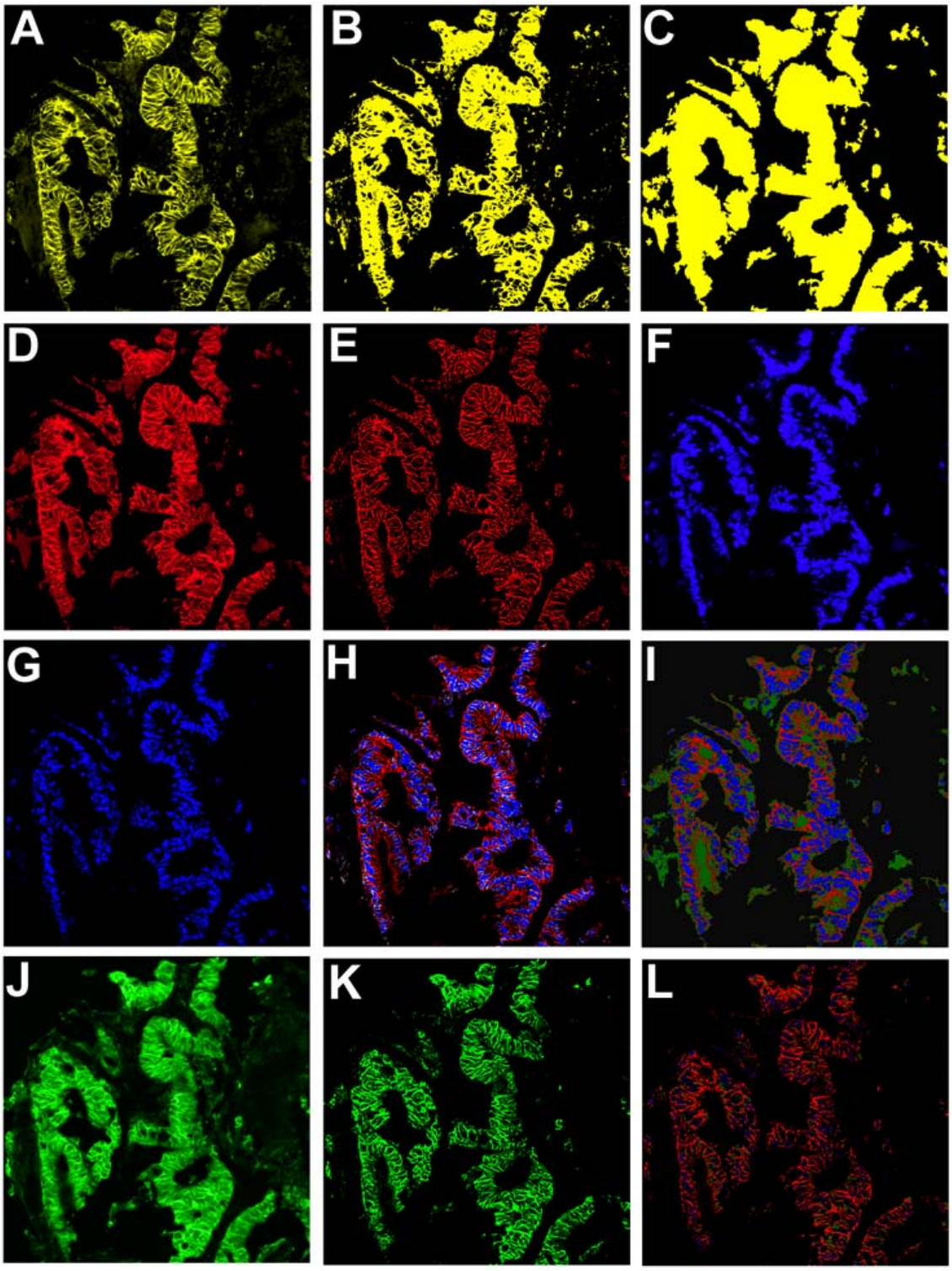

Fig. 2 Step-by-step methodology for RESA and PLACE algorithms. ***a***, Tumor cells are differentiated from stroma using a tumor-specific tag. Anti-cytokeratin is used to distinguish colon carcinoma from surrounding desmoplastic stroma. ***b***, The cytokeratin image is gated to form a binary mask. ***c***, The binary mask is enhanced by filling holes and removing small objects. ***d***, An image of the membrane-specific tag is taken. Anti-α-

catenin is used to tag the membrane of a colon carcinoma. ***e***, The membrane tag image is exponentially subtracted using RESA (Rapid Exponential Subtraction Algorithm). ***f***, An image of the nucleus-specific tag is taken. DAPI is used to tag the nuclei of a colon carcinoma. ***g***, The nuclear tag image is exponentially subtracted using RESA. ***h***, The membrane and nuclear tag images are merged, and overlapping pixels are identified and removed. White pixels represent overlap. ***i***, The membrane and nuclear compartments are overlaid on the tumor-specific mask. The overlay ensures that non-tumor nuclei and stroma are not included in the analysis of the target marker. ***j***, An image of the target-specific marker is taken, in this case, β-catenin expression of a colon carcinoma. ***k***, The target marker image is exponentially subtracted using RESA. ***l***, The intensity of the marker is divided into the various subcellular compartments. In this tumor, β-catenin is predominantly localized to the membrane (red) with minor amounts found in the nuclei (blue) and cytoplasm (green).

Table 1 Five-year multivariate analysis of survival

Variable	Relative Risk (95% C.I.)	*P*-value
Histologic Grade 3/3	1.100 (0.655–1.846)	0.7195
Nuclear Grade 3/3	1.096 (0.655–1.834)	0.7283
Age ^{3} 50 yrs	1.501 (0.791–2.850)	0.2140
Stage ^{3} iiia	**1.775 (1.051–2.998)**	**0.0318**
Low ER*	**2.566 (1.428–4.611)**	**0.0016**

Variables in boldface are statistically significant. *: Tumors with estrogen receptor (ER) levels in the bottom 25% were compared to tumors in the top 25%.

Table 2 Multivariate analysis of total nuclear and nuclear/membrane β-catenin ratios

	Total nuclear β-catenin*		Nuclear/membrane β-catenin†	
Variable	relative risk	*P*-value	relative risk	*P*-value
High β-catenin	1.118 (0.599–2.084)	0.7266	**1.865 (1.068–3.259)**	**0.0285**
TNM stage ^{3} T3	1.462 (0.926–2.309)	0.1033	1.527 (0.872–2.673)	0.1386
Nodal metastases	1.466 (0.963–2.227)	0.0739	1.490 (0.866–2.564)	0.1495
Poorly-differentiated	1.216 (0.624–2.032)	0.6929	1.490 (0.712–3.115)	0.2902
Age ^{3} _ 62-year old	**1.944 (1.162–3.252)**	**0.0113**	**2.412 (1.212–4.800)**	**0.0121**

Variables in boldface are statistically significant. *: Tumors with nuclear β-catenin levels in the top 10% were compared to the rest; †: tumors with nuclear/membrane β-catenin ratios in the top 25% were compared to the bottom 25%.

Table 3 Chi-square analysis of total nuclear and nuclear/membrane β-catenin ratios

	Total nuclear*	Nuclear/membrane ratio†
	***P*-value**	***P*-value**
TNM stage ^{3} T3	0.1622	0.7744
Presence of nodal metastases	**0.0136‡**	0.3979
Poorly-differentiated tumors	0.1392	0.9717
Age ^{3} 62-year old	0.8521	0.3459

Variables in boldface are statistically significant. *: Tumors with nuclear β-catenin levels in the top 10% were compared to the rest; †: tumors with nuclear/membrane β-catenin ratios in the top 25% were compared to the bottom 25%; ‡: 70% of tumors with high nuclear β-catenin were node-positive versus 41% of tumors with lower levels.

Table 4 Partial list of markers successfully analyzed using the RESA and PLACE algorithms

Marker	Source	Dilution	Predominant pattern(s)
EGFR	CST	1:50	nuclear, membrane
Phospho-EGFR (Y1068)	CST	1:50	nuclear, membrane
Phospho-EGFR (Y1045)	CST	1:50	membrane, cytoplasmic
Phospho-EGFR (Y845)	CST	1:50	nuclear, membrane
Phospho-EGFR (Y992)	CST	1:50	membrane, cytoplasmic
HER2/neu	DAKO	neat	membrane, cytoplasmic
Phospho-ERK (T202/Y204)	CST	1:100	nuclear, cytoplasmic
STAT3	CST	1:100	nuclear, cytoplasmic
Phospho-STAT3 (Y705)	CST	1:50	nuclear, cytoplasmic
KI-67	Trans.	1:250	nuclear
Na/K ATPase α1	Upstate	1:100	membrane
Laminin-beta 1	Upstate	1:100	peri-membranous
Heparan Sulfate	Seikagaku	1:50	peri-membranous
Alpha-catenin	BD	1:500	membrane
Beta-cateinin	BD	1:500	membrane, nucleus
Plakoglobin	BD	1:500	membrane
Cytokeratin AE1/AE3	DAKO	1:250	cytoplasmic
Cytokeratin polyclonal	Zymed	1:50	cytoplasmic
Spectrin	Yal e	1:50	membrane, cytoplasmic, nuclear
Survivin	Yale	1:100	cytoplasmic
CD44	BD	1:200	membrane

BD: BD Biosciences/Transduction Labs (San Diego, California); CST: Cell Signaling Technology (Beverly, Massachusetts); DAKO Corp (Carpenteria, California); Seikagaku America (Falmouth, Massachusetts); Upstate Biotech (Lake Placid, New York); Zymed (South San Francisco, California).